# Internship Report

## Implementation, validation and use of the TenStream Solver coupled to the Dutch Atmospheric Large-Eddy Simulation

Menno Veerman

26-08-2018

Internship done from 26-03-2018 to 27-07-2018 at the Ludwig-Maximilians-Universität München, Germany

## Supervisors

**Ludwig-Maximilians-Universität, Chair of Experimental Meteorology, Munich**
Dr. Fabian Jakub
Prof. Dr. Bernhard Mayer

**Wageningen University, Meteorology and Air Quality Group, Wageningen**
Prof. Dr. Jordi Vilà-Guerau de Arellano
Xabier Pedruzo-Bagazgoitia MSc

**Abstract**

Althought radiative transfer is an important atmospheric process, it is often solved in one dimension only. While the use of 1D radiative transferwq schemes results in considerable savings of computational time, it neglects the horizontal transport of radiation. In this study, the TenStream radiative transfer solver was coupled to the Dutch Atmospheric Large-Eddy Simulation (DALES) to solve radiative transfer in 3D. The radiative fluxes and heating rates in the DALES-TenStream coupling are validated and the performance of the coupling is assessed. Subsequently, I used the TenStream solver to study the development of the boundary layer and the interaction between clouds and surface fluxes with 3D radiative transfer. In the validation part, the TenStream solver shows good agreement with two 1D radiative transfer solvers and correctly applied heating rates. However, the TenStream solver is over 20 times slower than the two 1D radiation schemes, but the difference in runtime may be reduced by further optimizing the coupling. To study the effects of solving radiative transfer in 3D, I conducted three simulations, using the TenStream solver and two 1D radiative transfer solvers. The simulations are based on a case with shallow cumulus developing in the afternoon over grassland, without horizontal wind or precipitation. It is found that using 3D radiative transfer results in stronger convection, thicker clouds and a higher cloud cover. Consequently, the incoming shortwave radiation and the surface heat fluxes are lower in the simulation driven by 3D radiation. However, due to the displaced cloud shadows, the sensible and latent heat fluxes beneath clouds are larger with 3D than with 1D radiative transfer, which also explains the stronger convection with 3D radiation. Conversely, the heat fluxes are lower in the cloud-shadowed areas with 3D radiative transfer. With a diurnal cycle of solar elevation angles up to about 37°, the simulations showed significant differences in the development of the boundary and clouds due to the neglection of horizontal energy transfer with 1D radiation. The results of this study show that solving radiative transfer in 3D may be necessary to accurately simulate the daily evolution of the atmosphere.

# Contents


**1 Introduction** **3**

**2 Model and case description** **4**

**3 Validation** **5**
3.1 Methods . . . . . 5
3.2 Results . . . . . 5

**4 Numerical performance** **8**
4.1 Methods . . . . . 8
4.2 Results . . . . . 8

**5 Effects of using 3D radiation on surface and atmosphere** **10**
5.1 Methods . . . . . 10
5.2 Boundary layer and cloud evolution . . . . . 10
5.3 Cloud-surface-radiation interaction . . . . . 13

**6 Numerical issues with humidity fields** **16**

**7 Discussion** **18**

**8 Conclusion** **21**

**References** **22**

# 1 Introduction

The radiative transfer of solar and thermal radiation is an important process in the atmosphere. Emission of thermal radiation near the cloud tops causes strong radiative cooling in the upper part of clouds, whereas there is moderate radiative warming near the cloud bottoms (Nishikawa *et al.*, 2004; Klinger *et al.*, 2017). Radiative heating due to the absorption of solar radiation in the upper part of clouds partially compensates the thermal radiative cooling (Nishikawa *et al.*, 2004; Jakub and Mayer, 2015). These radiative effects may influence the development of clouds by increasing condensation in regions with strong cooling and by enhancing turbulence within clouds (Guan *et al.*, 1997; Klinger *et al.*, 2017). Furthermore, radiation is an important component of the surface energy balance. Shadowing of the surface by clouds can therefore greatly reduce the surface sensible and latent heat fluxes (Lohou and Patton, 2014; Pedruzo-Bagazgoitia *et al.*, 2017).

In general circulation models and large-eddy simulations, radiative transfer is almost always solved in 1D. Most 1D radiative transfer solvers use two streams for energy propagation, one up- and one downward stream, which is computationally very efficient compared to 3D solvers (Jakub and Mayer, 2016) and can give reasonable results at low horizontal resolutions (OHirok and Gautier, 2005). However, 1D solvers do not account for the horizontal transfer of energy, thereby neglecting the displacement of clouds shadows and radiative heating or cooling at cloud sides (Jakub and Mayer, 2015). Recent studies (Gronemeier *et al.*, 2016; Jakub and Mayer, 2017) showed that these 3D effects may have a considerable impact on the development of clouds.

Besides the total incoming radiation at the surface, another important factor determining the surface heat and moisture fluxes is the partitioning between direct and diffuse radiation (Kanniah *et al.*, 2012; Pedruzo-Bagazgoitia *et al.*, 2017). Diffuse radiation is distributed more horizontally homogeneous and can reach deeper canopy layers more easily than direct radiation (Li *et al.*, 2014), which result in a higher photosynthesis rate and therefore more evapotranspiration. Using a large-eddy simulation with an additional multi-layer canopy radiative transfer scheme, Pedruzo-Bagazgoitia *et al.* (2017) found that the latent heat flux is largest beneath thin clouds due to increasingly diffuse radiation, whereas the sensible heat flux is largest in clear sky conditions, where the net radiative fluxes are highest. However, the enhanced latent heat flux under thin clouds is found using only 1D radiation (Pedruzo-Bagazgoitia *et al.*, 2017). It is not known whether this enhancement can still be observed with 3D radiation.

In this research, the effects of solving the radiative transfer in 3D, instead of 1D, on the atmosphere and the surface are studied using the Dutch Atmospheric Large-Eddy Simulation (DALES) (Heus *et al.*, 2010). The TenStream radiative transfer solver (Jakub and Mayer, 2015) is coupled to DALES to accurately solve the radiative transfer in 3D. A short description of the TenStream solver and of the case on which all simulations are based is provided in Section 2. The radiative transfer in the DALES-TenStream coupling is validated (Section 3) and the numerical performance of the TenStream solver compared to two 1D solvers is assessed (Section 4). Afterwards, in the main part of the research (Section 5), the effects of using 3D radiation on the development of the boundary layer and clouds as well as the interaction between the surface heat fluxes and clouds due to radiation are studied. Last, the occurrence of negative specific humidities in DALES is investigated (Section 6). The methods and results are discussed in Section 7 and a short conclusion is given in Section 8.

## 2 Model and case description

All experiments are performed with the Dutch Atmospheric Large-Eddy Simulation (DALES) (Heus *et al.*, 2010). DALES version 4.1 is used in this study, including an additional scheme for the radiative transfer of diffuse and direct radiation in a multi/layer canopy, which has been described and implemented in DALES by Pedruzo-Bagazgoitia *et al.* (2017). To accurately solve radiative transfer in three dimensions, DALES is coupled to the TenStream solver, developed and described by Jakub and Mayer (2015).

In the TenStream solver, three streams are used for direct radiation: downward and in both horizontal directions. Ten streams are used for diffuse radiation: upward and downward at the top and the bottom of each grid box and an upward and downward sideward stream at each of the four sides of each grid box. Optical properties are calculated with the Rapid Radiative Transfer Model (Mlawer *et al.*, 1997) and used to determine the transport coefficients that govern the radiative transfer in each stream. The transport coefficients are determined using a lookup table, precomputed with a Monte Carlo model for a range of values of each optical property and for various zenith angles. Last, the radiative fluxes in each direction are calculated and the heating rates are determined from the divergence of the radiative fluxes.

In the TenStream solver, it is possible to calculate only the spectral bands that have sufficiently changed between radiation time steps at each radiation time step[1]. With this adaptive scheme, all spectral bands all calculated at least every 300 seconds, but certain spectral intervals are not recomputed at intermediate time steps if the atmosphere has not changed. This adaptive scheme is only used in Section 5.

In addition to this full 3D solver (TenStream), two 1D radiative transfer solvers are used in this study: the 1D $\delta$-eddington solver (twostream) within the TenStream package and the Rapid Radiative Transfer Model for use in GCMs (RRTMG) that has already been implemented in DALES.

The initial and background conditions and the configuration of DALES are similar to Pedruzo-Bagazgoitia *et al.* (2017) and Vilà-Guerau de Arellano *et al.* (2014). The case represents a relatively warm late September day in the Netherlands, with shallow cumulus clouds developing in the early afternoon (Pedruzo-Bagazgoitia *et al.*, 2017). Precipitation is disabled and there is no background wind, but initially a weak horizontal wind (1 m s$^{-1}$) is present in the lowest vertical layers, which mostly dissappears before the first clouds are formed. The surface is interactive and the vegetation type is grass, covering 90% of the surface. The initial soil moisture content is 0.385 m$^3$ m$^{-3}$.

[1]This is termed adaptive spectral integration (not yet published).

# 3 Validation

## 3.1 Methods

As a first step, the coupling of the TenStream solver to DALES is validated. Three simulations are performed, with the TenStream and twostream solvers and with RRTMG. The size of the domain is only 3200 x 3200 x 5000 m$^3$, with a horizontal resolution of 100 x 100 m$^2$ and a vertical resolution of 50 m. The simulations are run for 10 hours, starting at 07:00 UTC (09:00 local time) and the radiation scheme is called every 300 seconds. The additional canopy radiative transfer scheme is switched off for the validation.

Firstly, I examine the radiative transfer through clouds and the application of the solar and thermal radiative heating rates in clouds. For this, a single time step is chosen with a sufficiently large cloud cover. Secondly, the coupling is validated by comparing height profiles of the horizontally averaged up- and downwelling radiation and the heating rates under clear-sky conditions. This is done only for the first radiation time step (07:05 UTC) so that the atmospheric states are still equal. Furthermore, the temporal evolutions of the average radiation at the surface and the domain top are compared.

## 3.2 Results

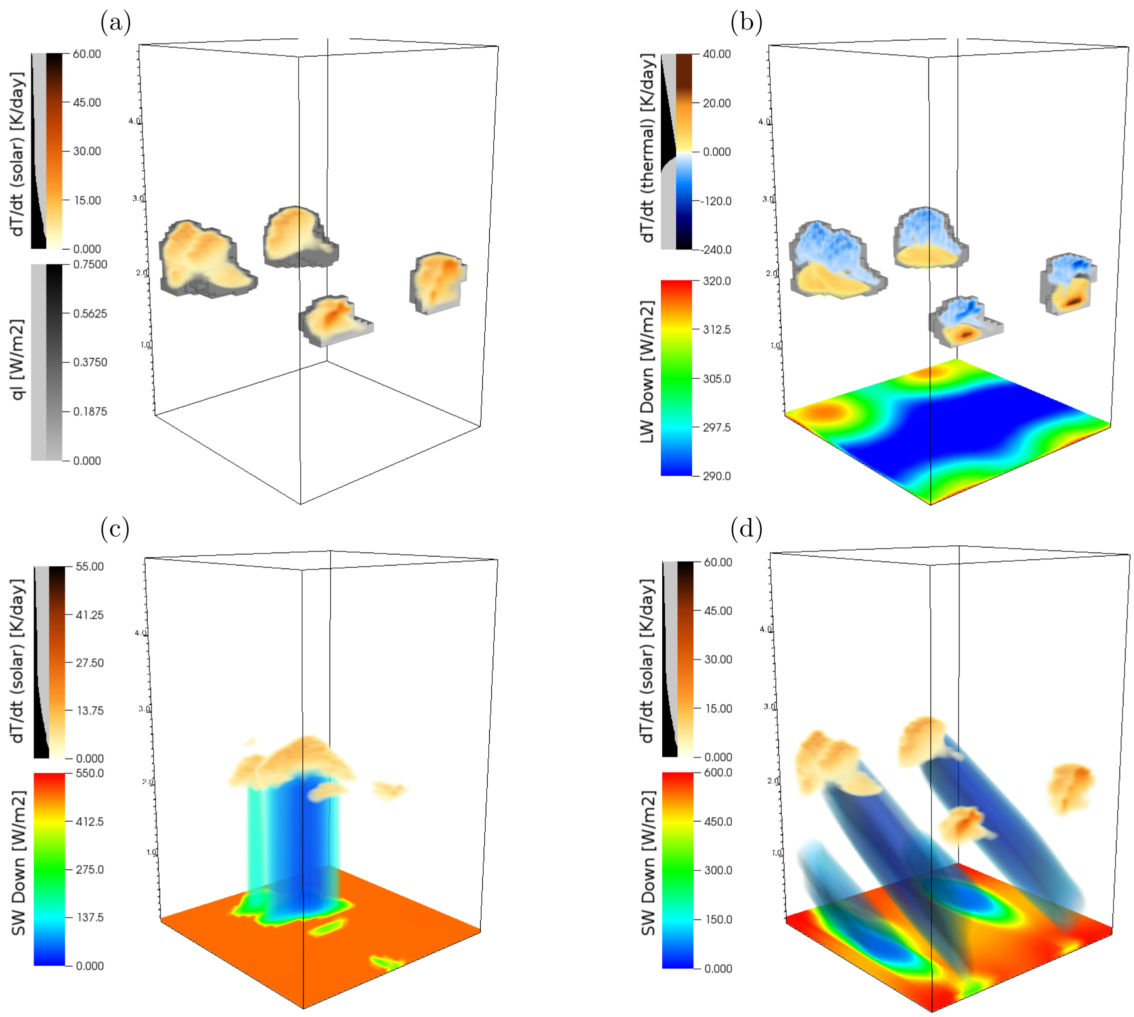


Figure 1: (a) Liquid water specific humidity ($q_l$) and solar heating rates (dT/dt). (b) Downward longwave radiation at the surface, thermal dT/dt and $q_l$ as in (a). (c), (d) Solar dT/dt and total (direct+diffuse) downward shortwave radiation (only lowest values shown above the surface layer).

The locations of the solar and thermal radiative heating rates correspond well to the locations of the clouds (Figure 1a,b). The solar heating rates are highest near the top of the clouds and decrease towards the cloud bottoms (Figure 1a). The mean downwelling shortwave radiation ($SW_{down}$) at the highest cloud layer (2675 m) is about 536 W m$^{-2}$, the liquid water content ($q_l$) ranges between 0 and 0.75 g kg$^{-1}$ and the solar heating rates are up to 60 K d$^{-1}$.

The thermal heating rates are strongly negative near the cloud tops and positive near the cloud bottoms (Figure 1b), indicating radiative warming in the lower and the radiative cooling in the upper parts of the clouds. The radiative cooling and warming by longwave radiation are in the ranges between -240 to 0 K d$^{-1}$ and 0 to 40 K d$^{-1}$, respectively. The downwelling longwave radiation ($LW_{down}$) at the surface is highest directly beneath the clouds, because clouds emit more longwave radiation than the clear sky, and gradually decreases from the cloudy towards the clear-sky areas (Figure 1b).

The effect of clouds on the radiative transfer of shortwave radiation is shown in Figures 1c and 1d for the RRTMG and TenStream simulations, respectively. Although the zenith angle is about 61.5°, the cloud shadows in the RRTMG simulation only extent vertically downward (Figure 1c). The sharp contrast in $SW_{down}$ between cloudy and clear-sky areas also shows the absence of horizontal energy transfer. The cloud shadows in the TenStream simulation (Figure 1d) extent downward under an angle, which clearly indicates the horizontal radiative transfer with 3D radiation. Furthermore, the gradually increase in $SW_{down}$ from the shaded towards the non-shaded areas shows the horizontal diffusion of radiation. Due to the relatively small domain, large zenith angle and periodic boundary conditions, the cloud shadows cross the domain boundary and re-enter the domain at the opposite boundary.

Vertical profiles of the horizontally averaged radiation and radiative heating rates at the first radiation time step (07:05 UTC) are shown in Figure 2. In each simulation, the downwelling shortwave radiation decreases by about 30 W m$^{-2}$ and the upwelling shortwave radiation by about 11 W m$^{-2}$ between the top and bottom of the domain (Figure 2a). The differences in shortwave radiation between the TenStream and twostream runs are very small, but in the RRTMG run the shortwave radiation is consistently about 5 W m$^{-2}$ higher. This bias may partly be caused by difference in the atmospheric background profiles: it was found that the differences in downwelling shortwave radiation at the top of the domain between various AFGL atmospheric constituent profiles (Anderson *et al.*, 1986) and the U.S. standard atmosphere 1976 (Anderson *et al.*, 1986), which has been used in this study, can be about 5 to 10 W m$^{-2}$. The solar heating rates are similar around the top and the bottom of the domain, but lower in the RRTMG run between roughly 1500 and 4000 m

The differences in the up- and downwelling longwave radiation between the runs are smaller than the differences in shortwave radiation (Figure 2b). At about half of the vertical levels, the thermal heating rates are quite similar as well. However, the thermal heating rates in the TenStream and twostream runs are higher than in RRTMG near the top of the domain, but lower around 3000 m and near the surface. As mentioned in Figure 2, however, these differences in thermal heating rates, as well as the differences in solar heating rates, could be because an atmospheric constituent is missing.

The time series of the up- and downwelling shortwave radiation and longwave radiation at the top of the domain are shown in Figures 3a and 3b, respectively. The temporal evolution of the downwelling radiation in the three simulations is very similar. The three time series of the upwelling radiation are also similar up to about 12:00 UTC, but differ slightly in the afternoon due to differences in the onset and development of clouds. The time series of the net radiation (Figure 3c) and the sensible and latent heat fluxes (Figure 3d) at the surface are very similar as well, apart from small differences between 12 and 16 UTC due to variations in cloudiness between the simulations.

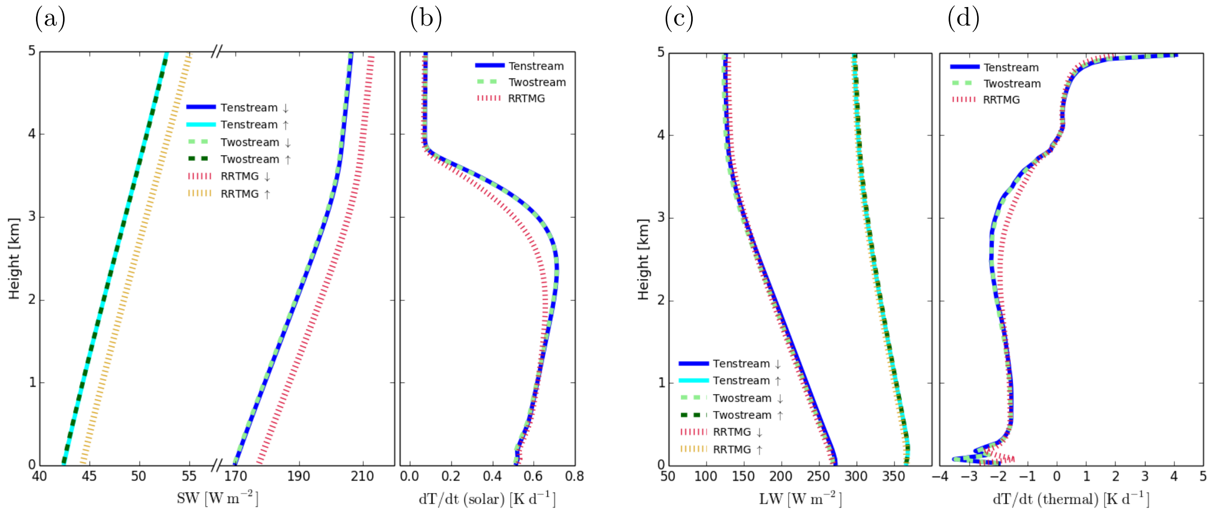


Figure 2: Vertical profiles of the up- and downwelling shortwave radiation (a), solar heating rates (b), up- and downwelling longwave radiation (c) and thermal heatings rates (d) for the RRTMG, Twostream and TenStream run at the first radiation time step (07:05 UTC). The differences between RRTMG and the TenStream and twostream solvers in (b) and (c) may be due to a missing tracer. This should be reinvestigated, but does not affect the results and conclusions of this study.

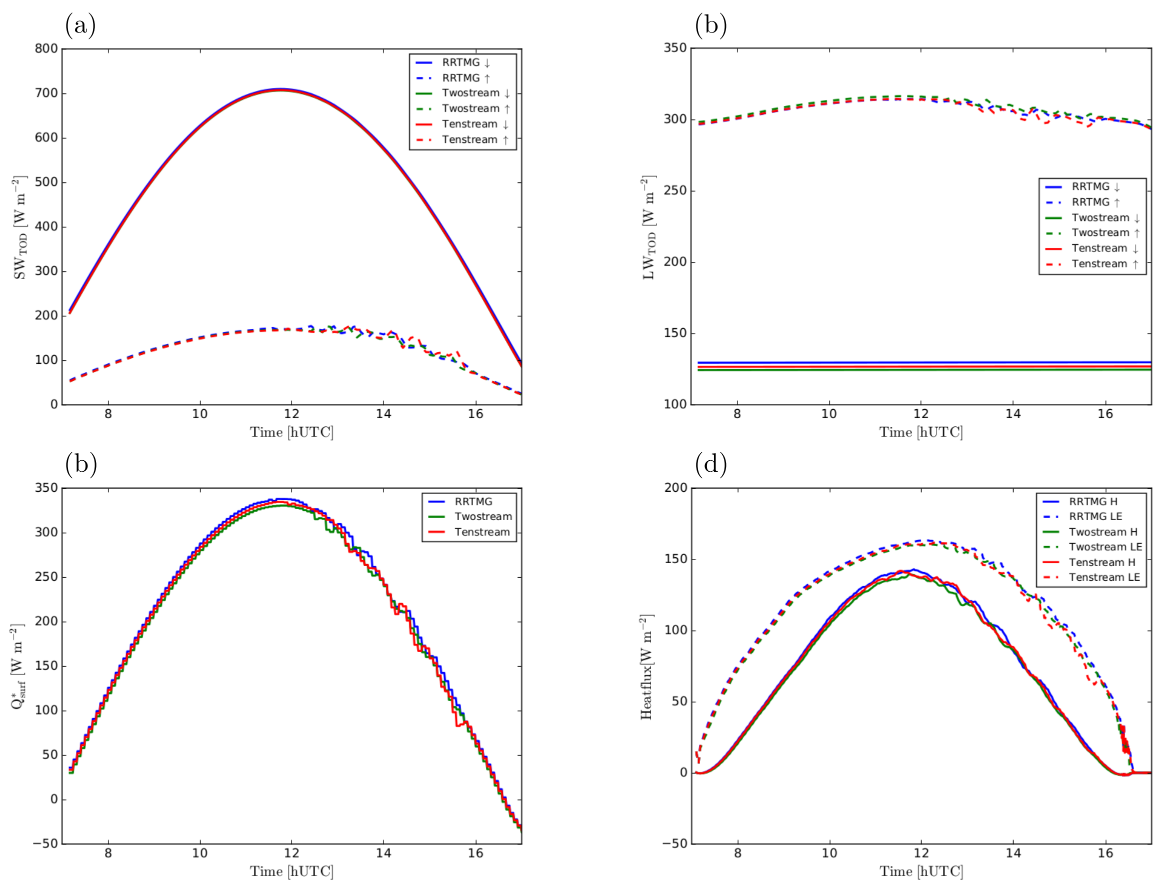


Figure 3: Time series of the up- and downwelling shortwave (a) and longwave (b) radiation at the top of the domain, the net radiation at the surface and the surface latent and sensible heat fluxes (d) in the RRTMG, twostream and TenStream runs.

# 4 Numerical performance

## 4.1 Methods

The numerical performance of the DALES-TenStream coupling is assessed to evaluate the extra computational costs required to have accurate 3D radiation in DALES with the TenStream solver. For this, the runtimes of the three main simulations (Section 5) are used. Additionally, several small simulations are performed to study the differences in runtime in more detail. The additional canopy radiative transfer scheme is not used here either and radiation is calculated every 300 seconds.

These additional simulations are also done with the TenStream and twostream solvers and with RRMTG. A horizontal domain size of 4800 x 4800 m is used, with a resolution of 200 x 200 m. The vertical domain size and resolution are as described in Section 3.1. Each simulation is run for only one hour, from 07:00 to 08:00 UTC, and the radiation scheme is called every 5 minutes. These simulations are performed at the Meteorogical Institute Munich (MIM) of the Ludwig-Maximilians-Universität (LMU) and on the Dutch supercomputer Cartesius, on only one node, but with a varying number of parallel tasks: 1, 2, 4, 5, 9, 12 and 16 tasks at LMU-MIM and 9, 12 and 24 tasks at Cartesius. A small overview of both systems is given in Table 1. Each run is repeated three times and only the minimum execution time is used for the analysis.

Table 1: Description of the computing nodes at of the Meteorological Institute Munich of the Ludwig-Maximilians-Universität (LMU-MIM) and of the Cartesius supercomputer: Number of cores, maximum number of processes (proc), CPU base frequency and the memory per node

| System | Cores | Proc | Frequency | Memory |
|---|---|---|---|---|
| LMU-MIM | 1x10 | 20 | 2.3 GHz | 54 GB |
| Cartesius | 2x12 | 24 | 2.6 GHz | 64 GB |

## 4.2 Results

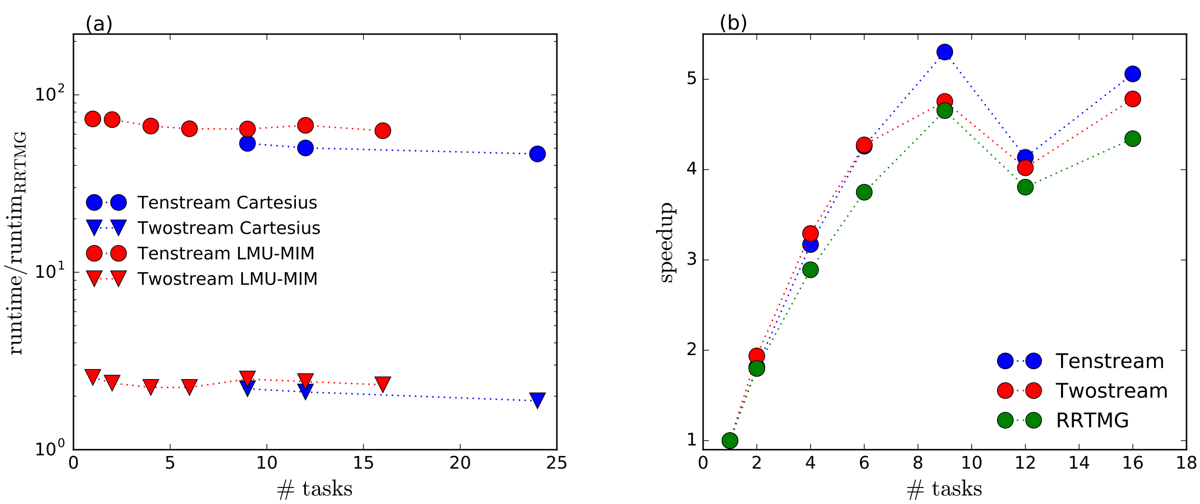


Figure 4: (a) Ratio of the runtime of the TenStream and twostream simulations to runtime of the RRTMG simuliation at Cartesius and the LMU-MIM against the number of tasks used for the same job. (b) Speedup of the TenStream, twostream and RRTM simulations at the LMU-MIM against number of tasks for the same job size.

The runtimes of the TenStream and twostream simulations compared to the RRTMG simulation are shown in Figure 4a, for different numbers of tasks on the Cartesius supercomputer and at the LMU-MIM. Here, the runtime is the time needed to complete one hour in the simulation. The twostream simulation is

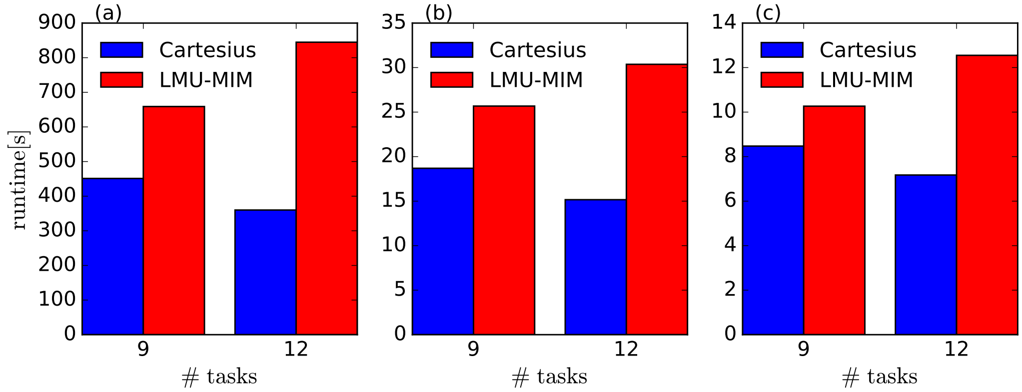


Figure 5: Runtime of the TenStream (a), twostream (b) and RRTMG (c) simulations using 9 or 12 tasks, on Cartesius and at the LMU-MIM

about 2 to 3 slower than the RRTMG simulation and the TenStream simulation is between approximately 40 and 80 times slower than the RRTMG simulation and roughly between 20 to 30 times slower than the twostream simulation. Figure 4a also shows that, on Cartesius, the ratio of the runtime of the TenStream and twostream simulations to the runtime of the RRTMG simulation slightly decreases as the number of tasks is increased.

The speedup achieved by using more tasks is higher for TenStream than for twostream and RRTMG (Figure 4b). At the LMU-MIM, the highest speedup of the TenStream and RRTMG simulations is achieved with 9 tasks on one node, which is the highest number of cores tested here for which only one task per core is used. The absolute runtimes of the simulations are shown in Figure 5, with either 9 or 12 tasks on Cartesius and at the LMU-MIM. As is also shown in Figure 4a, twostream is about 2.5 times slower than RRTMG and TenStream is over 20 times slower than twostream. On Cartesius, the runtime of each simulation is lower with 12 than with 9 tasks. At the LMU-MIM, the runtime is higher with 12 than with 9 tasks (Figure 5) as was also shown by Figure 4b.

The total wall time of the full twostream simulation is 11622 s, whereas the total wall time of the TenStream simulation is 130052 s. This is an increase in runtime of only about 11 times. This lower runtime difference is largely because, in the TenStream simulation, not all spectral bands are calculated at each time step during which the radiation scheme is called.

# 5 Effects of using 3D radiation on surface and atmosphere

## 5.1 Methods

As the main part of this research, the effects of using 3D radiation on the evolution of the boundary layer and clouds and on the surface heat fluxes in the presence of clouds are studied. Three simulations are performed with the three radiation schemes mentioned in Section 2. A horizontal domain of 9.6 x 9.6 km is used, with a resolution of 100 x 100 m. The height of the domain is 5472 m, with a vertical resolution of 12 m. Here, the canopy radiative transfer scheme of Pedruzo-Bagazgoitia *et al.* (2017) is used to have a more accurate response of the surface heat fluxes on changes in the incoming direct and diffuse radiation. The simulations are run for 10 hours, between 07:00 UTC and 17:00 UTC, and local time is UTC+2. The solar elevation angle has a diurnal cycle and reaches up to about 37°. Here, the radiation scheme is called every 30 seconds to better represent the interaction between clouds and radiation and the adaptive spectral integration scheme is used to reduce the runtime of the TenStream simulation.

Firstly, the focus is on the domain averaged boundary layer height and macrophysical cloud properties, such as cloud top and bottom, cloud cover, liquid water path and the vertical moisture fluxes within clouds. Secondly, the interaction between the surface heat fluxes and clouds through radiation is considered. For this, the latent and sensible heat fluxes beneath clouds and in cloud shadows are studied.

## 5.2 Boundary layer and cloud evolution

The temporal evolution of domain-averaged boundary layer height in the three simulations is shown in Figure 6a. Here, the atmospheric boundary layer (ABL) height at each grid point is defined as the first height at which the vertical gradient of the liquid water potential temperature ($\theta_l$) is equal to half of the maximum $\theta_l$ gradient between the surface and the top of the domain (Pedruzo-Bagazgoitia *et al.*, 2017; Ouwersloot *et al.*, 2011). In the RRTMG simulation, the ABL height is slightly higher than in the twostream simulation throughout the simulation. The ABL height in the TenStream simulation is similar to the ABL height in RRTMG and twostream until about 13:30 UTC, but decreases with time afterwards. This decrease in TenStream is mainly the result of an increasing area with a strong temperature inversion near the surface (not shown). These temperature inversions are due to strong cooling of the surface, caused both by a low amount of incoming shortwave due to the displacement of cloud shadows with 3D radiative transfer and by emission of longwave radiation to clear sky.

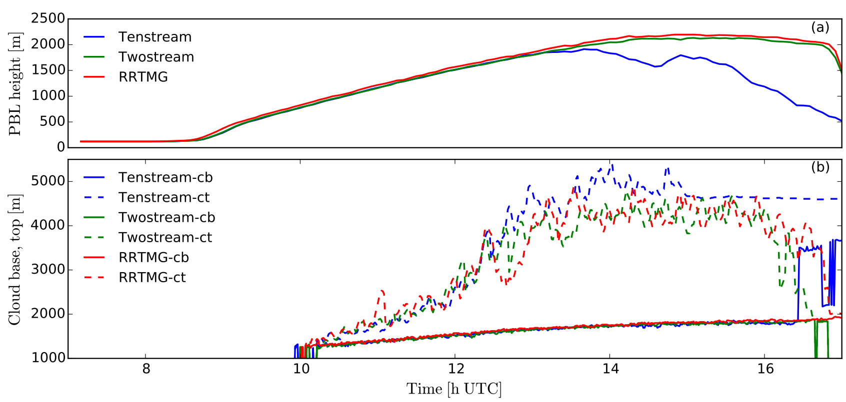


Figure 6: Timeseries of (a) the average boundary layer height and (b) the cloud base (cb) and cloud top (ct) for the TenStream, twostream and RRTMG simulations

The heights of the cloud bases in the three simulations are very similar up to about 16:15 UTC (Figure 6b). The cloud tops in both the RRTMG and the twostream simulation are around 4000 to 4500 m, whereas the clouds tops in the TenStream simulation reach over 5000 m. The high cloud bases and cloud tops near the end of the simulation indicate that a high cloud layer ($\approx$ 3500 − 4500 m) remains in the TenStream simulation, whereas the low clouds near the ABL top are dissolving at the end of all simulations.

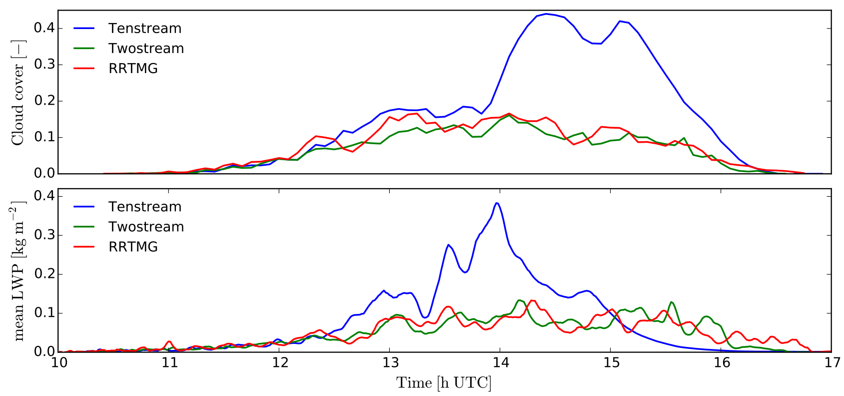


Figure 7: Timeseries of (a) the cloud cover and (b) the mean liquid water path (LWP), averaged over the cloud-covered columns, for the TenStream, twostream and RRTMG simulations. Columnss are considered cloud covered if the LWP is larger than 10 g $m^{-2}$

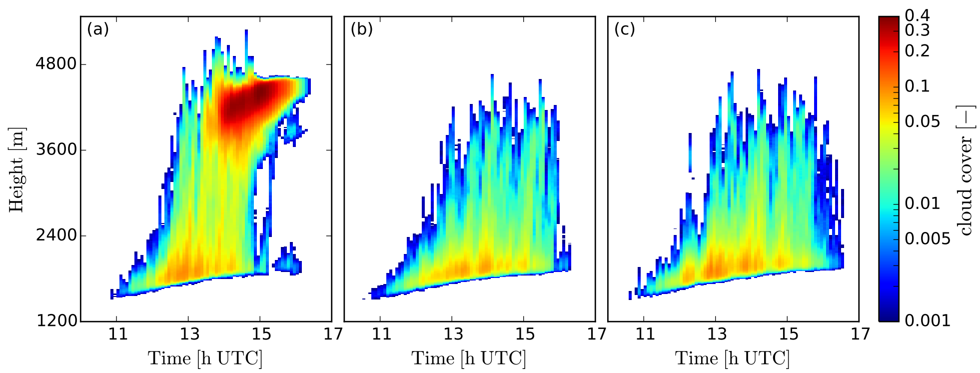


Figure 8: Vertical cross-section of the horizontal cloud cover at each height level against time for the TenStream (a), twostream (b) and RRTMG (c) simulations.

The cloud cover in the RRTMG and twostream simulations are statistically indistinguishable, between 10% and 20% during the middle of the day (Figure 7a). In the TenStream simulation, however, the cloud cover is much higher (>40%), especially after 14:00 UTC (Figure 7a). This higher cloud cover in TenStream is not necessarily because much more shallow cumulus are formed, but rather due to individual clouds being wider than in the other two simulations (not shown). The mean liquid water path (LWP), averaged only over the locations where clouds are present, is also quite similar in the RRTMG and twostream simulations (Figure 7b), fluctuating around 0.1 kg $m^{-2}$ between 13:00 and 16:00 UTC. Until 15:00 UTC, the mean LWP in the TenStream simulation is much higher than in the simulations with 1D radiation, almost reaching 0.4 kg $m^{-2}$. Using the TenStream solver thus results in larger and thicker clouds, which suggests that there is stronger convection beneath the clouds.

The highest cloud covers in the TenStream simulation occur after the peak in the mean LWP. Additionally, the mean LWP after 15:00 UTC is lower in the TenStream simulation than in the RRTMG or twostream simulations, whereas the cloud cover is still higher in the TenStream simulation (Figure 7). Both indicate the high cloud cover in the TenStream simulation can be largely associated with the formation of a rather thin cloud layer at high elevations that remains after the strong convection around 14:00 UTC. This is shown in more detail in Figure 8. At the cloud bottoms, the cloud cover in the three simulations is quite similar ($\approx 5 - 10\%$). Near the cloud tops, however, the cloud cover in the TenStream simulation is much higher than in the other two simulations after about 14:00 UTC. These high cloud covers around $4000 - 4500$ m in the TenStream simulation are likely the result of horizontal spreading of the thickest clouds near their cloud tops and remain after the decrease in cloud cover near the cloud basess around 15:00 UTC.

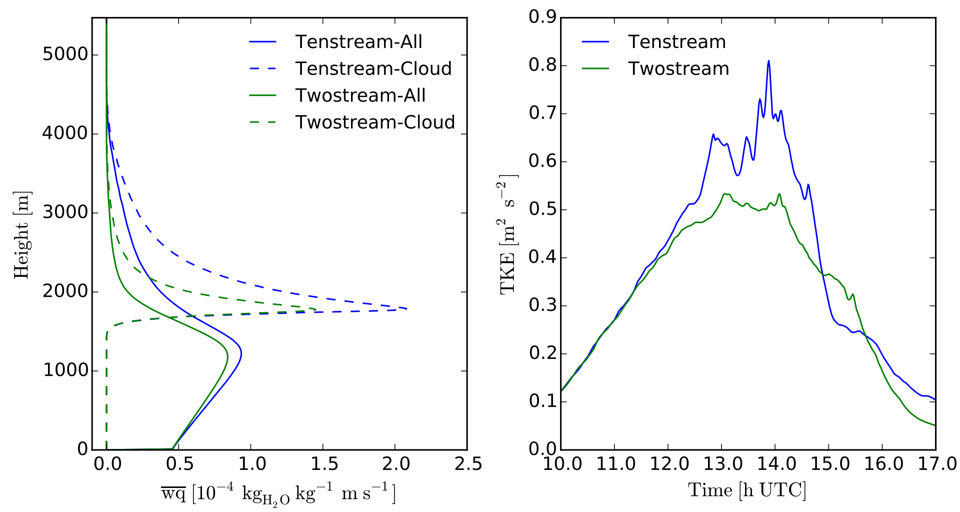


Figure 9: (a) Vertical profiles of the vertical moisture flux for the TenStream and twostream simulations, averaged between 11:00 and 13:00 UTC over either all grid points (All) at eich height level or only the grid points containing liquid water (Cloud). (b) Timeseries of the domain-averaged turbulent kinetic energy (TKE) for the TenStream and twostream simulations.

The stronger convection in the TenStream simulation is also shown by the vertical moisture flux (Figure 9a). The mean vertical moisture fluxes, averaged over all horizontal grid points, are higher in the TenStream simulation than in the twostream case at most heights, indicating that more moisture is transported upwards. The differences in vertical moisture flux between the TenStream and twostream simulations are larger when only the moisture fluxes within clouds are considered (Figure 9a). The higher moisture fluxes within clouds in the TenStream simulation indicate the presence of stronger updrafts, resulting in the higher cloud tops. Between roughly 12:00 and 15:00 UTC, the vertically averaged turbulent kinetic energy (TKE) is also higher in the TenStream case (Figure 9b). This higher TKE indicates that there are stronger turbulent motions in the TenStream simulation, which can also be related to the higher moisture fluxes in the TenStream case.
The timeseries of the horizontally averaged total downwelling shortwave radiation ($SW_{tot}$) at the surface, as well as its diffuse and direct components, are shown in Figure 10a. In the first half of simulation, the incoming shortwave radiation is very similar in the TenStream and twostream simulations. After 12:00 UTC, however, $SW_{tot}$ is lower in the TenStream than in the twostream simulation. This lower $SW_{tot}$ is mostly due to a strong decrease in direct radiation ($SW_{dir}$), which is only partly compensated by an increase in diffuse radiation ($SW_{dif}$). The lower $SW_{dir}$ and higher $SW_{dif}$ in the TenStream simulation may be largely explained by the higher cloud cover.

The temporal evolutions of the domain averaged surface sensible (H) and latent (LE) heat fluxes (Figure 10b) are similar to that of $SW_{tot}$ (Figure 10a): In the first half of simulation, H and LE in the TenStream and twostream simulations are almost equal, whereas H and LE are lower in the TenStream simulation during most of the afternoon. These lower heat fluxes could be expected, since $SW_{tot}$ is lower as well in the TenStream simulation. Although the shift from $SW_{dir}$ to $SW_{dif}$ can be beneficial for plants, which may increase the evapotranspiration despite the lower $SW_{tot}$ (Pedruzo-Bagazgoitia *et al.*, 2017), the lower LE in the TenStream simulation indicates that the higher $SW_{dif}$ is not enough to compensate the lower $SW_{tot}$ during most of the afternoon.

## 5.3 Cloud-surface-radiation interaction

As shown in Section 5.2, the average surface heat fluxes are lower in the TenStream than in the twostream case, whereas the higher LWP and cloud cover in the TenStream simulation indicate stronger convection, which may seem contradictory. It is therefore also interesting to study the spatial distribution of the surface heat fluxes in relation to the clouds in more detail. Figure 11 shows the sensible and latent heat fluxes as a function of liquid water path, where H and LE are grouped into several bins of LWP and subsequently averaged per bin.

Under clear sky (LWP $\leqslant$ 1 g m$^{-2}$), both heat fluxes are on average higher in the twostream than in the TenStream simulation. Under all cloudy conditions (LWP $>$ 1 g m$^{-2}$), especially at large LWPs, H and LE are higher in the TenStream case, which can be attributed to the horizontal energy transfer with 3D radiation: In contrast to the two simulations with 1D radiations, the cloud shadows in the TenStream simulation, the areas with reduced $SW_{dir}$ due to scattering and absorption by the clouds, are not necessarily located beneath the clouds. The cloudy areas in the TenStream simulation may thus receive high amounts of both $SW_{dif}$ and $SW_{dir}$, whereas $SW_{dir}$ is always reduced beneath clouds in the twostream simulation, so less energy is available for surface heating and evapotranspiration.

In twostream, H decreases with increasing LWP and is highest under clear sky. The maximum LE, however, is at LWPs of about 10 g m$^{-2}$, similar to the enhanced evapotranspiration under thin clouds due to an increase in $SW_{dif}$ reported by Pedruzo-Bagazgoitia *et al.* (2017). In the TenStream simulation, both H and LE increase with increasing LWP for LWP up to about 300 g m$^{-2}$ because of the enhanced $SW_{dif}$. For higher LWPs, however, both heat fluxes decrease, which is presumably because near the end of time period used for Figure 11 (11-13 UTC), when the highest LWPs occur, the cloud configuration is such that several cloud shadows are beneath neighbouring clouds

The sensible heat flux is approximately as strong as the latent heat flux under clear sky conditions, in both the TenStream and twostream simulations. Under all clouds (LWP $>$ 1 g m$^{-2}$, LE is larger than H in twostream, presumably because share of $SW_{dif}$ in $SW_{tot}$ is higher beneath clouds than under clear sky. In the TenStream simulation, however, H is larger than LE for most LWPs, even though $SW_{dif}$ is enhanced beneath the clouds, which may indicate that the share of $SW_{dif}$ increases less with increasing LWP than in twostream: $SW_{dir}$ is often not reduced beneath clouds in the TenStream simulation due to the displaced cloud shadows and in the TenStream case $SW_{dif}$ beneath clouds is on average lower than in twostream because of the sideward scattering of shortwave radiaton.

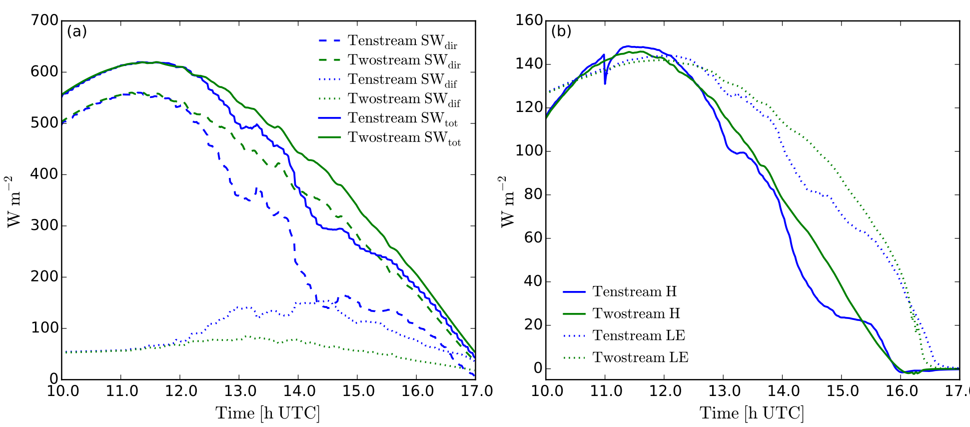


Figure 10: Timeseries of (a) the incoming total ($SW_{tot}$), direct ($SW_{dir}$) and diffuse ($SW_{dif}$) shortwave radiation at the surface and (b) the surface sensible (H) and latent (LE) heat flux for the TenStream and twostream simulations. The jump in H and LE at around 11:00 UTC in the TenStream simulation is because of a restart of the TenStream simulations at this time.

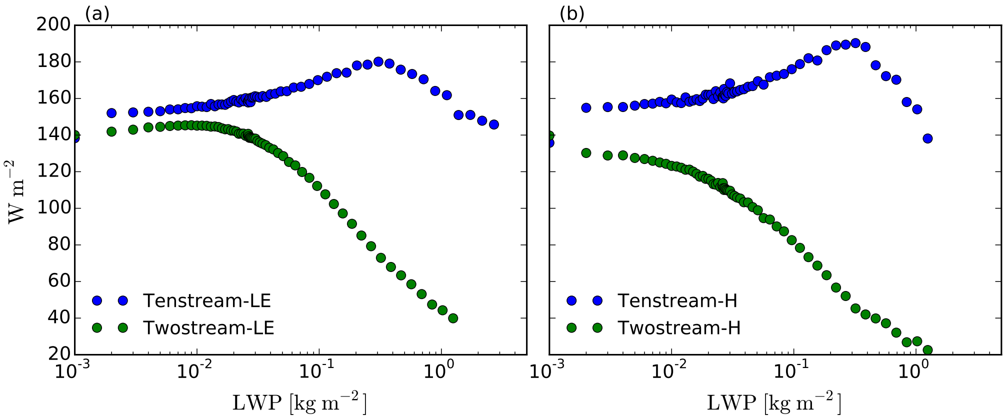


Figure 11: Latent heat flux (a) and sensible (b) heat flux against liquid water path (LWP), averaged per LWP bin between 11:00 and 13:00 UTC, for the TenStream and twostream simulations

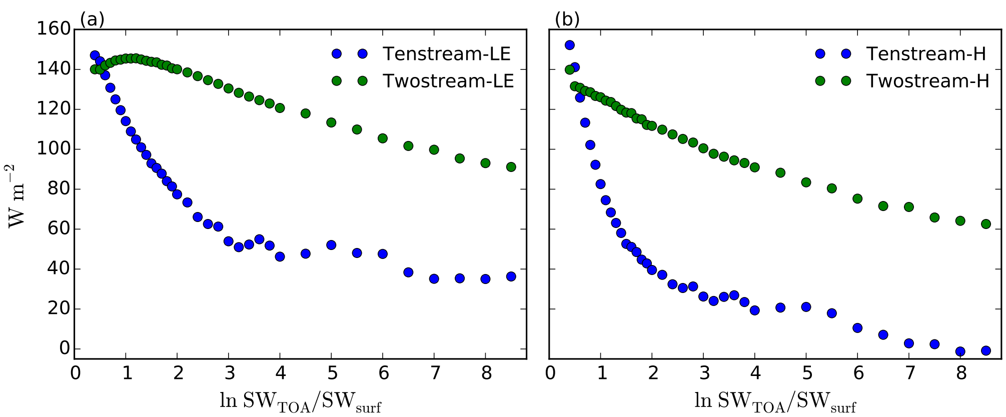


Figure 12: Latent heat flux (a) and sensible (b) heat flux against the natural logarithm of the ratio of the incoming shortwave radiation at the top of the atmosphere ($\mathrm{SW_{TOA}}$) and the direct radiation at the surface ($\mathrm{SW_{surf}}$). The heat fluxes are averaged per $\ln\frac{\mathrm{SW_{TOA}}}{\mathrm{SW_{surf}}}$-bin, between 11:00 and 13:00 UTC, for the TenStream and twostream simulations. $\ln\frac{\mathrm{SW_{TOA}}}{\mathrm{SW_{surf}}}$ is used as an approximation of the optical depth in the direction of the incoming direct radiation at the surface.

Since the cloud covered areas in the TenStream simulation do not necessarily correspond to the cloud-shadowed areas, as is the case with 1D radiative transfer, it is also interesting to study the heat fluxes as a function of optical depth. Because the optical depth along the slanted path of the sun rays is not readily available, I estimate it from the inverse of Lambert-Beer's law, i.e.

$$\tau = \ln\frac{\mathrm{SW_{TOA}}}{\mathrm{SW_{surf}}}, \tag{1}$$

where $\mathrm{SW_{TOA}}$ is the incoming shortwave radiation at the top of atmosphere and $\mathrm{SW_{surf}}$ is the direct shortwave radiation at the surface. In general, H and LE decrease with increasing optical depth in both simulation due to the lower $\mathrm{SW_{tot}}$ (Figure 12), although LE is at a maximum at an optical depth of about 1, which corresponds to the enhanced evapotranspiration under thin clouds (Figure 11, Pedruzo-Bagazgoitia *et al.* (2017)). The absence of this LE maximum in the TenStream simulation and the lower heat fluxes for most optical depths indicate that in the TenStream asimulation decrease in $\mathrm{SW_{dir}}$ in the cloud shadows is compensated less by an increase in $\mathrm{SW_{dif}}$ than in the twostream simulation. This is because the cloud shadows in the TenStream simulation are often located under clear sky and consequently receive little diffuse radiation due to scattering by clouds.

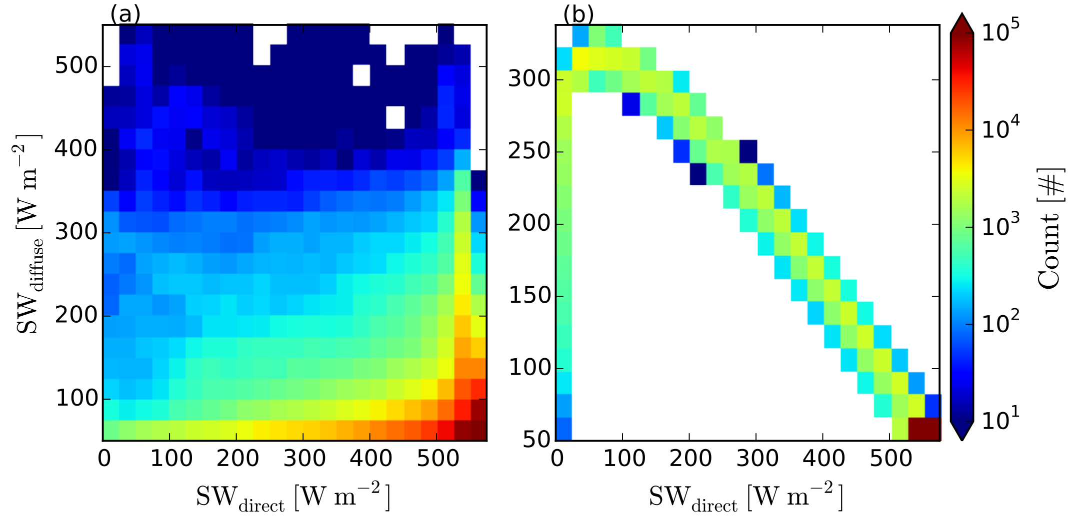


Figure 13: 2D histograms of partitioning of direct ($SW_{dir}$) and diffuse ($SW_{dif}$) shortwave radiation at the surface between 11:00 and 13:00 UTC for the TenStream (a) and twostream (b) simulations. In (b), the bottom right corner in represents clear-sky conditions (high $SW_{dir}$) and the cloud thickness increases first towards the top left corner (increasing $SW_{dif}$, decreasing $SW_{dir}$) and then towards the bottom left corner (low $SW_{dif}$ and $SW_{dir}$ beneath very thick clouds).

The degree to which a decrease in $SW_{dir}$ is compensated by an increase in $SW_{dif}$ is thus an important factor determining the heat fluxes beneath clouds and in cloud shadows. As shown in Figure 13, surface grid points with low $SW_{dif}$ and high $SW_{dir}$, representing the non-shaded areas, are most common. In the twostream simulation, there is a clear negative correlation between $SW_{dir}$ and $SW_{dif}$, except at very low $SW_{dir}$. In the TenStream simulation, however, such a correlation is absent, since a decrease in $SW_{dir}$ can correspond to both a low and a high $SW_{dif}$ (Figure 13a). That is, the cloud shadows on the surface can be located both under clear sky and beneath clouds, although under clear sky is more frequent. Conversely, Figure 13a also indicates that cloudy areas are most often not shaded by other clouds, therefore receiving the same $SW_{dir}$ as under clear sky in twostream and more $SW_{dif}$ due to overhead clouds.

# 6 Numerical issues with humidity fields

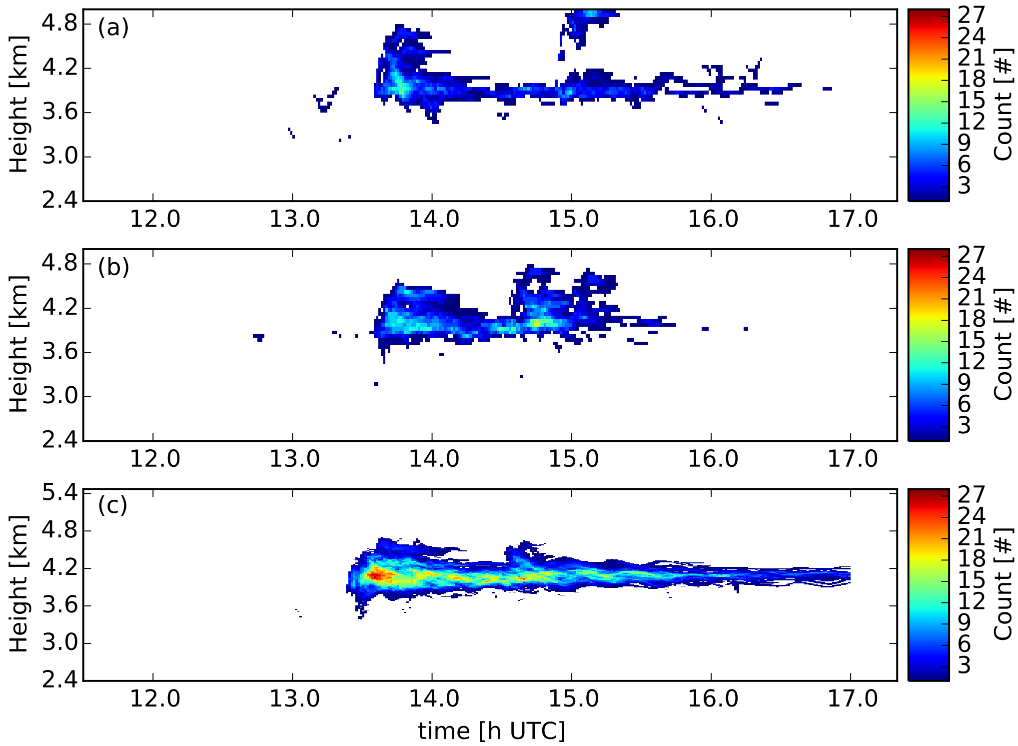


Figure 14: Vertical distribution of the number of negative water vapour contents as function of time for the 1-sec (a), 20-sec (b) and 12m-vert (c) simulations (see Table 2). The water vapour content is calculated as the difference between the total and liquid water specific humidity at the start of the radiation scheme.

I observed that DALES tends to produce unrealistically low and high temperatures and negative specific humidities in most simulations, which causes the simulations to crash. These crashes are presumably caused by negative water vapour contents entering the radiation scheme, resulting in unrealistic heating rates. These negative water vapour contents, calculated as the difference between the total specific humidity and the liquid water content, are mostly due to negative total specific humidities. We tried to solve this issue during my internship, but due to time limitations we continued by setting a lower threshold of $10^{-18}$ $\mathrm{kg_{H_2O}\ kg^{-1}}$ for the water vapour contents, which was already done for the RRTMG radiation scheme in DALES. We are confident that this lower threshold does not reduce the ability to draw conclusions from the results of this study. It must be noted that this lower boundary is only set within the radiation scheme. The negative specific humidities are allowed to exists in the rest of the model. We assume that these negative values do not affect the simulation significantly. Furthermore, setting a lower boundary to the total specific humidity may cause problems in the conservation of moisture.

Nevertheless, it is interesting to study the occurrences of the negative water vapour contents. Four additional simulations are performed, with a similar set-up as described in section 3.1. but using a horizontal domain size of 3600 x 3600 m, a horizontal resolution of 300 x 300 m and the RRTMG radiation scheme. The simulations have either a different maximum solution time step of 1 s (1-sec) or 20 s (20-sec), a higher vertical resolution of 12 m (12m-vert), or use only a first order advection scheme (adv-1). A short overview of the four simulations is given in Table 2

The number of occurrences of a negative water vapour content is 5608 in the 20-sec simulation, 4160 in the 1-sec simulation, 54361 in the 12m-vert simulation and only 2 in the adv-1 simulation. Decreasing the maximum solution time step thus reduces the number of amount of occurrence. Increasing the vertical res-

Table 2: Summary of the differences in the numerical set-up of the four runs performed to study the negative specific humidities in DALES. For each of the four runs are given the number of vertical levels (vert levels), with resolution (res) between brackets, the maximum time step ($dt_{max}$) and the advection scheme (adv). The advection schemes are either first order upwind (1) or fifth order horizontally and second order vertically (52).

| run | vert levels(res) | $dt_{max}$ | adv |
|---|---|---|---|
| 20-sec | 100 (50 m) | 20 s | 52 |
| 1-sec | 100 (50 m) | 1 s | 52 |
| 12m-vert | 456 (12 m) | 20 s | 52 |
| adv-1 | 100 (50 m) | 20 s | 1 |

olution seems to result in more occurrences per vertical level, since the number of vertical levels is about 4.5 times higher whereas the number of occurrences is approximately 9.7 times higher. Using only $1^{st}$ order advection reduces the number of occurrences significantly, although this advection scheme is less accurate.

The number of negative water vapour contents against height and time is shown in Figure 14 for the 20-sec, 1-sec and 12m-vert simulations. The negative water vapour contents start occurring around 12:30 UTC (20-sec) or 13:30 UTC (1-sec, 12m-vert) and the number of occurrences is highest between roughly 13:30 UTC and 15:00 UTC (20-sec) or 16:00 UTC (1-sec, 12m-vert), when the cloud cover and cloud thickness are highest. The negative water vapour contents are mostly concentrated near the cloud tops, around 4000-4200 m. The maximum number of occurrences per height and per time step is 27, which is quite large compared to the total number of horizontal grid points (144).

# 7 Discussion

First of all, I validate the DALES-TenStream coupling with three small simulations, using the 1D $\delta$-eddington (twostream) and the full 3D (TenStream) radiative transfer solvers of the TenStream package and the RRTMG radiation scheme already implemented in DALES. In the three validation simulations, the time series of the radiation at the top of the atmosphere and at the surface are very similar. The vertical profiles of the clear-sky shortwave and longwave radiative fluxes and heating ratings are similar as well, apart from a small bias of the up- and downwelling shortwave radiation in TenStream and twostream with respect to RRTMG. The reason of this bias is not exactly known, but possible causes are the differences in atmospheric background profiles or the different versions of the RRTMG code in DALES and the RRTMG code used in the TenStream solver for the optical properties. However, since the bias is quite small and approximately constant over the whole vertical profile, it is assumed to have little influence on any differences in the daily evolution of the atmosphere between the simulations.

The radiative heating rates within clouds in the TenStream simulations are similar to the heating rates reported by e.g. Jakub and Mayer (2015) and Klinger *et al.* (2017) in terms of magnitude and spatial distribution (Section 3), thus indicating a correct application of the heating rates in DALES-TenStream. The time series of the net radiation at the surface and of the surface heat fluxes in the three validation simulations are very similar, which may be surprising, since it would suggest that using 3D radiation has only little influence on the evolution of the atmosphere. However, the effects of having 3D radiation have likely been suppressed in the validation simulations by the small domain size, which caused several clouds to shade themselves due to cloud shadows crossing the domain boundaries, and because the radiation scheme is called only once every 300 seconds.

Second of all, I determine the runtimes of several short simulations, with the twostream and TenStream solvers and with RRTMG, to asses the numerical performance of the DALES-TenStream coupling (Section 4). The simulations with the TenStream solver are about 20 to 30 times slower than the simulations with the twostream solver. This difference in runtime is larger than the differences reported by Jakub and Mayer (2016) and may be reduced by using a different matrix preconditioner (Jakub and Mayer, 2016). The differences in runspeed between the TenStream and twostream solvers can also be reduced by not solving all spectral bands at each radiation time step. The runtimes of the simulations with the twostream solver are between 2 to 3 times larger than the runtimes of the RRTMG simulations. The DALES-TenStream coupling is not optimized for numerical performance yet, so there is still room for improvement.

Third of all, I perform three simulations to study the effects of using 3D radiative transfer on the development of the atmosphere in DALES (Section 5), with a larger domain size and a higher vertical resolution than the validation simulations and using an additional canopy radiative transfer scheme (Pedruzo-Bagazgoitia *et al.*, 2017). The evolution of the boundary layer and of the cloud properties in the two simulations with 1D radiation is very similar (Section 5.2). In the simulation with 3D radiative transfer, the height of the clouds tops, the cloud cover and the cloud liquid water path are much higher than with 1D radiation. Such an increase in cloud cover and LWP has also been reported by (Jakub, 2016).

There are also significant differences in cloud development between the simulations: in twostream and RRTMG, numerous shallow cumulus develop and dissolve continously and near the end of the simulations all clouds have dissolved. In the TenStream simulation, some clouds become much larger and thicker than the shallow cumulus and spread horizontally near the cloud tops. This leaves a thin cloud layer, at some point too thin to be counted in the cloud cover, which remains until the end of the simulation. The higher, thicker clouds also indicate that in the TenStream simulation there is stronger convection beneath and within clouds, which is also suggested by the higher vertical moisture fluxes and the stronger turbulence in the TenStream run. However, It should be noted that precipitation is disabled. Given the thickness of the clouds in the TenStream simulation, it is not unlikely that precipitation would have occurred (Geoffroy *et al.*, 2008). Precipitation could have resulted in a lower cloud cover and a lower mean LWP by reducing the cloud liquid water content, but may also induce cold-pool dynamics, which can result in thicker clouds (Schlemmer and Hohenegger, 2014).

Due to the higher cloud cover and LWP, the total incoming shortwave radiation reaching the surface is on average lower in the TenStream than in the twostream simulation, which in turn results in lower domain-averaged heat fluxes in the TenStream simulation. Despite the preference of photosynthesis in canopy for diffuse radiation (Li *et al.*, 2014), the latent heat release in the TenStream simulation is lower than in the twostream simulation. This indicates that the increase in diffuse shortwave radiation in the TenStream simulation does not compensate the decrease in total shortwave radiation sufficiently.

The thicker clouds in the TenStream case may seem in contrast with the lower surface fluxes, but can be attributed to differences in the spatial distribution of the heat fluxes in relation to clouds between the simulations (Section 5.3). Under clear sky, the heat fluxes in the TenStream and twostream simulations are quite similar. In the twostream simulation, the sensible heat flux almost continously decreases with increasing LWP. The latent heat flux, however, first slightly increases with increasing LWP for LWPs up to about 10 g $m^{-2}$ and only decreases with increasing LWP for higher LWPs, which is similar to the findings of Pedruzo-Bagazgoitia *et al.* (2017). In the TenStream simulation, however, both the sensible and latent heat flux increase with increasing LWP for LWPs up to about 300 g $m^{-2}$. Under all clouds (LWP $> 1$g $m^{-2}$), the surface heat fluxes are thus lower in the twostream than in the TenStream simulation. This is because with 1D radiation, the cloud shadows are always located directly beneath the clouds, which always results in less direct shortwave radiation reaching the surface and therefore lower surface heat fluxes.

For most optical depths, the heat fluxes in the cloud shadows are on average higher in the twostream than in TenStream simulation. This is because the cloud shadows in the TenStream simulation are often not located directly beneath a cloud, so the reduced direct radiation is often compensated less by an increase in diffuse radiation than in twostream. It should be noted that in this study the optical depth is approximated using the ratio of the shortwave radiation at the top of the atmosphere to the direct shortwave radiation at the surface. This approximation underestimates the optical depth due to the Delta-scaling of the optical properties (Joseph *et al.*, 1976). This underestimation may partly explain why in this study the latent heat flux is highest at optical depths of about 1, whereas Pedruzo-Bagazgoitia *et al.* (2017) reported a maximum around optical depths of 2 by using optical depths based on liquid water path and effective droplet radius.

These differences in the effects of clouds on the surface heat fluxes indicate that by using 1D radiation, the heat fluxes are on average underestimated beneath clouds and overestimated under clear sky. The lower heat fluxes beneath the clouds in twostream likely inhibit further growth of the clouds, which causes the lower mean LWP and the lower vertical moisture fluxes within clouds in the twostream simulation. It must be noted that in these simulations, the horizontal background wind is close to zero. With a sufficiently high horizontal wind speed, the feedback between the surface fluxes and clouds may be different (Lohou and Patton, 2014). However, Gronemeier *et al.* (2016) and Jakub and Mayer (2017) have already shown that, even with considerable background winds, the effects of solving radiative transfer in 3D may still influence the development of clouds.

Part of the surface moisture flux is the tranpiration of plants, the loss of water through the plants stomata. Since both $H_2O$ and $CO_2$ are exchanged with the atmosphere through the stomata of plants, the evapotranspiration at the surface can be related to the carbon assimilation of plants (Pedruzo-Bagazgoitia *et al.*, 2017). Although the assimilation was not studied specficially, it can be assumed that the results concerning the latent heat flux are similar for the carbon assimilation. On a local scale this means that with 3D radiation, the assimilation is on average higher beneath clouds and lower under clear sky than with 1D radiation. On a more regional scale, the average assimilation is lower with 3D radiation due to the higher in cloud thickness and cloud cover.

To reduce computational time, especially with 3D radiation, a relatively small horizontal domain size (9.6 km) and coarse horizontal resolution (100 m) is used compared to the studies of Pedruzo-Bagazgoitia *et al.* (2017) and Vilà-Guerau de Arellano *et al.* (2014), on which the case used in this study is based. This small domain size and coarse resolution may be insufficient to accurately represent the cloud fields, especially for the deeper convection in the TenStream simulation. It is not known to which degree moisture is conserved in the simulations, but it is found that negative specific humidities and negative water water vapour contents are sometimes produced by DALES. To prevent negative water vapour contents in the radiation scheme, which would result in unrealistic radiative heating rates, all negative water vapour contents are set to $10^{-18}$ $\mathrm{kg_{H_2O}\ kg^{-1}}$. This correction is not applied to the negative specific humidities outside of the radiation scheme, because it might cause errors in the conservation of moisture.

# 8 Conclusion

In this study, the Dutch Atmospheric Large-Eddy Simulation (Heus *et al.*, 2010) is coupled to the TenStream 3D radiative transfer solver (Jakub and Mayer, 2015). The radiative transfer and radiative heating rates are validated and the numerical performance of the DALES-TenStream coupling is assessed. Furthermore, the effects of using 3D radiation instead of 1D radiation on the evolution of the atmosphere and on the radiation-induced interaction between clouds and the surface are studied. Despite a small bias in the shortwave radiation at the top of the domain, the validation shows a good agreement between the TenStream and twostream solvers of the TenStream package and RRTMG, as well as a correct application of the radiative heating rates with TenStream solver.

It is found that the cloud cover and liquid water path in the simulation with 3D radiative transfer are higher than in the simulations with 1D radiative transfer, whereas the boundary layer near the end of the simulation is lower. This indicates that using 3D radiative transfer results in thicker clouds and stronger convection, which is also suggested by the higher vertical moisture fluxes in the simulation with 3D radiative trasfer. Due to the higher cloud cover and thicker clouds, the incoming shortwave radiation at the surface is lower in the simulation with 3D radiative transfer, which in turn causes the lower surfaces sensible and latent heat fluxes.

The surface heat fluxes underneath clouds are higher in the simulation with 3D radiative transfer than in the simulations with 1D radiative transfer. On the shadowed surface areas, however, the surface heat fluxes are on average higher with in the simulation with 3D radiative transfer for most optical depths. Both differences can be attributed to the fact that, with 3D radiative transfer, the cloud shadows are not necessarily located beneath clouds. The direct shortwave radiation is therefore often not reduced beneath clouds when the radiative tranfer is solved in 3D, whereas the reduced shortwave radiation on the shadows surface areas is often not compensated by an increase in diffuse radiation. Although there is a large difference in runspeed between the simulations with 3D and 1D radiation, the results of this study suggest that solving radiative transfer in 3D may be necessary to accurately represent the surface heat fluxes in the presence of clouds.

To better understand the effects of solving radiation in 3D instead of 1D, the interactions between clouds and the surface heat fluxes with 3D radiative transfer should be in more detail. I recommended for further research to study the effect of using 3-D radiative transfer under a wide range of surface surface conditions or with a high horizontal wind speed.

# References


Anderson GP, Clough SA, Kneizys F, Chetwynd JH, Shettle EP. 1986. Afgl atmospheric constituent profiles (0.120 km). Technical report, AIR FORCE GEOPHYSICS LAB HANSCOM AFB MA.

Geoffroy O, Brenguier JL, Sandu I. 2008. Relationship between drizzle rate, liquid water path and droplet concentration at the scale of a stratocumulus cloud system. *Atmospheric Chemistry and Physics* **8**(16): 4641–4654, doi:10.5194/acp-8-4641-2008.

Gronemeier T, Kanani-Sühring F, Raasch S. 2016. Do shallow cumulus clouds have the potential to trigger secondary circulations via shading? *Boundary-Layer Meteorology* **162**(1): 143–169, doi:10.1007/s10546-016-0180-7.

Guan H, Yau MK, Davies R. 1997. The effects of longwave radiation in a small cumulus cloud. *Journal of the Atmospheric Sciences* **54**(17): 2201–2214, doi:10.1175/1520-0469(1997)054⟨2201:TEOLRI⟩2.0.CO;2.

Heus T, van Heerwaarden CC, Jonker HJJ, Pier Siebesma A, Axelsen S, van den Dries K, Geoffroy O, Moene AF, Pino D, de Roode SR, Vilà-Guerau de Arellano J. 2010. Formulation of the dutch atmospheric large-eddy simulation (dales) and overview of its applications. *Geoscientific Model Development* **3**(2): 415–444, doi:10.5194/gmd-3-415-2010.

Jakub F. 2016. On the impact of three dimensional radiative transfer on cloud evolution, available at http://nbn-resolving.de/urn:nbn:de:bvb:19-197226 (last access 14-8-2018).

Jakub F, Mayer B. 2015. A three-dimensional parallel radiative transfer model for atmospheric heating rates for use in cloud resolving modelsthe tenstream solver. *Journal of Quantitative Spectroscopy and Radiative Transfer* **163**: 63 – 71, doi:10.1016/j.jqsrt.2015.05.003.

Jakub F, Mayer B. 2016. 3-d radiative transfer in large-eddy simulations - experiences coupling the tenstream solver to the ucla-les. *Geoscientific Model Development* (4): 1413–1422.

Jakub F, Mayer B. 2017. The role of 1-d and 3-d radiative heating in the organization of shallow cumulus convection and the formation of cloud streets. *Atmospheric Chemistry and Physics* **17**(21): 13 317–13 327, doi:10.5194/acp-17-13317-2017.

Joseph JH, Wiscombe WJ, Weinman JA. 1976. The delta-eddington approximation for radiative flux transfer. *Journal of the Atmospheric Sciences* **33**(12): 2452–2459, doi:10.1175/1520-0469(1976)033⟨2452:TDEAFR⟩2.0.CO;2.

Kanniah KD, Beringer J, North P, Hutley L. 2012. Control of atmospheric particles on diffuse radiation and terrestrial plant productivity: A review. *Progress in Physical Geography: Earth and Environment* **36**(2): 209–237, doi:10.1177/0309133311434244.

Klinger C, Mayer B, Jakub F, Zinner T, Park SB, Gentine P. 2017. Effects of 3-d thermal radiation on the development of a shallow cumulus cloud field. *Atmospheric Chemistry and Physics* **17**(8): 5477–5500, doi:10.5194/acp-17-5477-2017.

Li T, Heuvelink E, Dueck TA, Janse J, Gort G, Marcelis LFM. 2014. Enhancement of crop photosynthesis by diffuse light: quantifying the contributing factors. *Annals of Botany* **114**(1): 145–156, doi:10.1093/aob/mcu071.

Lohou F, Patton EG. 2014. Surface energy balance and buoyancy response to shallow cumulus shading. *Journal of the Atmospheric Sciences* **71**(2): 665–682, doi:10.1175/JAS-D-13-0145.1.

Mlawer EJ, Taubman SJ, Brown PD, Iacono MJ, Clough SA. 1997. Radiative transfer for inhomogeneous atmospheres: Rrtm, a validated correlated-k model for the longwave. *Journal of Geophysical Research: Atmospheres* **102**(D14).

Nishikawa T, Maruyama S, Sakai S. 2004. Radiative heat transfer analysis within three-dimensional clouds subjected to solar and sky irradiation. *Journal of the Atmospheric Sciences* **61**(24): 3125–3133, doi:10.1175/JAS-3268.1.

OHirok W, Gautier C. 2005. The impact of model resolution on differences between independent column approximation and monte carlo estimates of shortwave surface irradiance and atmospheric heating rate. *Journal of the Atmospheric Sciences* **62**(8): 2939–2951, doi:10.1175/JAS3519.1.

Ouwersloot HG, Vilà-Guerau de Arellano J, van Heerwaarden CC, Ganzeveld LN, Krol MC, Lelieveld J. 2011. On the segregation of chemical species in a clear boundary layer over heterogeneous land surfaces. *Atmospheric Chemistry and Physics* **11**(20): 10 681–10 704, doi:10.5194/acp-11-10681-2011.

Pedruzo-Bagazgoitia X, Ouwersloot HG, Sikma M, van Heerwaarden CC, Jacobs CMJ, de Arellano JVG.

2017. Direct and diffuse radiation in the shallow cumulusvegetation system: Enhanced and decreased evapotranspiration regimes. *Journal of Hydrometeorology* **18**(6): 1731–1748, doi:10.1175/JHM-D-16-0279.1.

Schlemmer L, Hohenegger C. 2014. The formation of wider and deeper clouds as a result of cold-pool dynamics. *Journal of the Atmospheric Sciences* **71**(8): 2842–2858, doi:10.1175/JAS-D-13-0170.1.

Vilà-Guerau de Arellano J, Ouwersloot HG, Baldocchi D, Jacobs JCM. 2014. Shallow cumulus rooted in photosynthesis. *Geophysical Research Letters* **41**(5): 1796–1802, doi:10.1002/2014GL059279.